JMEPEG
https://doi.org/10.1007/s11665-022-06697-5

1059-9495/$19.00

TECHNICAL ARTICLE

Effect of Intermetallic Compounds on the Microstructure, Mechanical Properties, and Tribological Behaviors of Pure Aluminum by Adding High-Entropy Alloy

Qinglin Li, Zhaobo Qiao, Xuepeng Bao, Chenglong Fan, Yefeng Lan, and JiQiang Ma

Submitted: 22 July 2021 / Revised: 6 December 2021 / Accepted: 25 December 2021

A novel aluminum matrix composites (AMCs) reinforced by multiphase intermetallic compounds were fabricated through a conventional casting approach. The microstructure, compression properties and tribological behavior of the AMCs were detailed studied by the scanning electron microscope (SEM), x-ray diffraction (XRD), and electron probe microanalysis (EPMA). The results demonstrated that the fraction of precipitated multiphase intermetallic compounds gradually increased with the increase of high-entropy alloy (HEA) adding content, and the grain size of α-Al obviously was reduced. The irregular multiphase intermetallic compounds, such as $Al_{70}Cr_{20}Ni_{10}$ and AlTiCrSi, are distributed in the Al matrix. However, the Al_2Cu and Al_7Cu_4Ni distributed in inter-dendrites of α-Al. In addition, the compression strength of AMCs reinforced by 20.0 wt.% HEA addition was significantly enhanced to 530 MPa due to the precipitation of multiphase intermetallic compounds. Meanwhile, its compression strain was higher than 25%. Compared with pure Al, the microhardness of AMCs was extremely increased to 160 HV when the addition content of HEA was up to 20.0 wt.%. When the addition amount of HEA reached 10.0 wt.%, the COF of the ACMs was decreased by 51.6% from 0.766 to 0.371. When the HEA content was up to 20.0 wt.%, the wear rate reached the minimum of 4.87×10^{-5} $mm^3/N{\cdot}m$, which was reduced by 31.9% compared with pure Al. Furthermore, the strengthening effect and wear mechanism of AMCs reinforced by HEA addition was also discussed.

Keywords aluminum matrix composites, high-entropy alloy, intermetallic compounds, mechanical properties, tribological properties

1. Introduction

Metal matrix composites (MMCs) are prepared by introducing reinforcement with certain mass fraction into matrix alloys. In recent years, aluminum matrix composites (AMCs) have attracted great interest of numerous scholars due to many excellent properties such as high specific strength and specific modulus, superior wear resistance, light weight and low thermal expansion coefficient. Therefore, the AMCs are widely used in aerospace and automobile manufacturing fields to substitute for traditional aluminum alloys (Ref 1-4). The particles (Ref 5, 6), fibers (Ref 7), and whiskers (Ref 8) act as the different reinforcements to enhance the properties of aluminum alloys. Generally, the ceramic particles reinforced AMCs exhibit higher specific strength, elastic modulus, and superior elevated-temperature performance (Ref 9-12). In addition, compared with pure aluminum or aluminum alloys, the reinforced AMCs have higher hardness, wear-resistance, and deformation resistance (Ref 13).

The high entropy alloys (HEAs), consisted of five or more elements in an equiatomic or near equiatomic, was proposed by Yeh et al. in 2004. These researches showed that the HEAs present extremely high hardness, exceptional elevated temperature strength, and superior compressive properties (Ref 14, 15). Recently, Laplanche et al. (Ref 16) found that the HEAs and metal matrix have extremely close thermal expansion coefficients, and there is the absence of phase transformation during cooling. Hence, the high entropy alloy particles (HEAp) can be regarded as the candidates for the reinforcement to strengthen aluminum alloys. Praveen Kumar et al. (Ref 17) indicated that the yield strength of AA 2024-15.0 wt.% HEAp composites was remarkably enhanced from 207 to 406 MPa, and the Vicker's hardness also was improved significantly. In addition, the previous study indicated that the both coefficient of friction (COF) of composites and the mass fraction of HEAp have a negative correlation (Ref 18). Yuan et al. (Ref 19) successfully fabricated AMCs by introducing HEAp into 2024 Al alloys through spark plasma sintering (SPS). It was found that the hardness (127.78 HV) of the AMCs increased by 63.7% compared with the unreinforced 2024 Al alloys (78.26 HV). The compression strength of 2024 Al alloy reinforced by $Al_3FeCrCoNi$ HEAp was up to 710 MPa (Ref 20). The compression strength and elongation of AMCs, manufactured

Z. Qiao and Q. Li have contributed equally to this work.

Qinglin Li, Zhaobo Qiao, Chenglong Fan, Yefeng Lan, and **JiQiang Ma**, State Key Laboratory of Advanced Processing and Recycling of Nonferrous Metals, School of Materials Science and Engineering, Lanzhou University of Technology, Lanzhou 730050, China; **Xuepeng Bao**, Jiuquan Iron and Steel (Group) Co. Ltd, Jiayuguan 735100, China. Contact e-mails: liql301@mail.nwpu.edu.cn, baoxp1995@163.com, 2770733913@qq.com.

Published online: 29 March 2022

by introducing $Al_{0.25}Cu_{0.75}FeNiCo$ HEA into 7075 Al alloy via mechanical alloying technology were 436.7 MPa and 11.42%, which were increased by 19.8% and 36.6%, respectively. Meanwhile, the elastic modulus of AMCs also was improved by 12.2% from 71.2 to 79.9 GPa (Ref 21). Lately, it was reported that the 12.0 vol.% CoCrFeNi/5083 composites were prepared by friction deposition technique. Karthik et al. (Ref 22) observed that there was the absence of precipitated intermetallic compounds on the interface between reinforcement (CoCrFeNi) and matrix (5083 Al alloys), and the yield strength and ductility obviously increased comparing with 5083 alloys. Furthermore, the compressive strength of $Al_{0.6}CoCrFeNi/Al_{65}Cu1_{6.5}Ti_{18.5}$ composites, prepared by spark plasma sintering (SPS), was increased by nearly 83.5% from 1700 ± 80 to 3120 ± 80 MPa (Ref 23). Similarly, Chen et al. (Ref 24) fabricated 10.0 wt.% and 20.0 wt.% AlCoCrFeNi/Cu composites by powder metallurgy. The result showed that the interface between HEAp and Cu matrix has no reaction product, and the compressive strength was significantly improved. In addition, Al matrix composites with Al_3Ni and Al_3Ti intermetallic compounds reinforcement have been reported (Ref 25, 26). Besides, it proved from our previous studies that the intermetallic compounds can be formed after introducing the AlCoCrFeNiTi HEA into pure Al, which is beneficial for the tensile properties of pure Al (Ref 27).

As a consequence, the AlSiTiCrNiCu HEA was chosen as the raw materials to prepare the Al matrix composites with multi-phases intermetallic compounds through the conventional casting approach. The purpose of the present work is to discuss the relationship between microstructure, mechanical properties and friction behavior of AMCs by adding AlSiTiCrNiCu HEA to pure Al melting.

Table 1 Chemical composition of pure Al, wt.%

Fe	Si	Mn	Mg	Zn	Cu	Al
0.28	0.13	0.10	0.10	0.0044	0.0013	Bal

2. Experiment Details

Al, Si, Ti, Cr, Ni and Cu elements with the purity of 99. 9% are used as raw materials to fabricate HEA by smelting in vacuum arc furnace filled with high purity argon atmosphere. The prepared AlSiTiCrNiCu HEA samples were melted repeatedly 4-5 times to ensure the uniformity of chemical composition (Ref 28).

The pure Al was selected as the matrix material, and its chemical composition is listed in Table 1. The pure Al was placed in graphite crucibles to heat and melt by resistance furnace at 760 °C. Meanwhile, the well-fabricated AlSiTiCrNiCu HEA (5.0, 10.0, 15.0, and 20.0 wt.%) was preheated to 800 °C. The pure Al was completely melted at 800 °C, and then, the preheated HEA was added into the aluminum melt according nominal addition concentration. In order to promote the dissolution of HEA in the aluminum melt, the melt was stirred every 5 min until the HEA completely melted to Al melting. The melt was degassed by hexachloroethane (C_2Cl_6) after being kept at 800 °C for 30 min.

Five groups metallographic specimens were taken from the same position of the as-cast rods and etched with Keller's reagent. The microstructure of composites was characterized by optical microscopy (OM, VHX-1000) and scanning electron microscope (SEM, JSM-6700F). Simultaneously, the x-ray diffraction instrument (D/max-2400) and electron probe micro-analysis (EPMA) were used to analyze the phases in AMCs.

In order to investigate the mechanical properties of AMCs, the compression specimens (the length of 20 mm and the diameter of 10 mm) were machined according to the GB/T

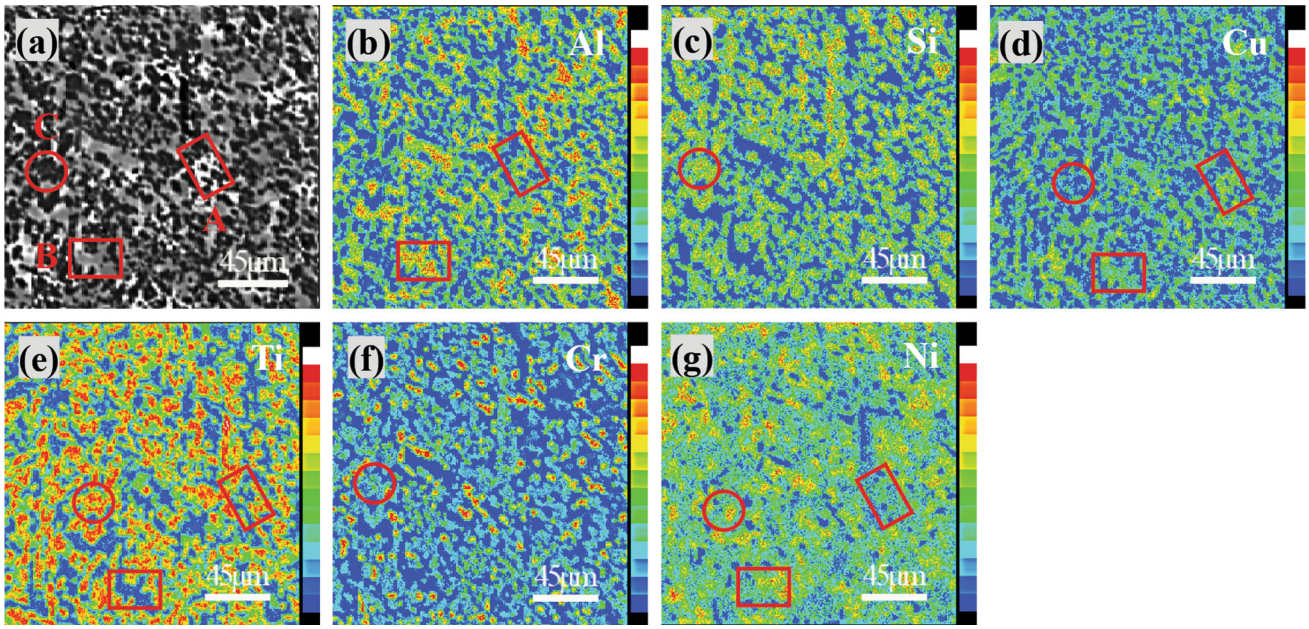

Fig. 1 EPMA analysis of AlSiTiCrNiCu HEA: (a) back-scattered electron image; (b) Al element; (c) Si element; (d) Cu element; (e) Ti element; (f) Cr element; (g) Ni element

7314-2005. The compression experiment was carried out by the material tensile testing machine (speed: 0.5 mm/min; temperature: 25 °C). The microhardness was measured by Micro Vickers Hardness Tester (0.1 kg of load and 10 s of dwell time). In addition, the friction specimens (the diameter of 12 mm and the length of 3 mm) were prepared from the pure Al and AMCs to assess the tribological properties of various AMCs. And then, the completed dry sliding friction on the HT-1000 high-speed circular motion friction tester was conducted under certain conditions (slide rate of 0.15 m/s, load of 10N, slide time of 30 min and temperature of 25 °C). Particularly, according to the test machine regulations, choose 316L small steel ball (the hardness of steel ball is 265HV) and friction specimens as a pair of friction pairs.

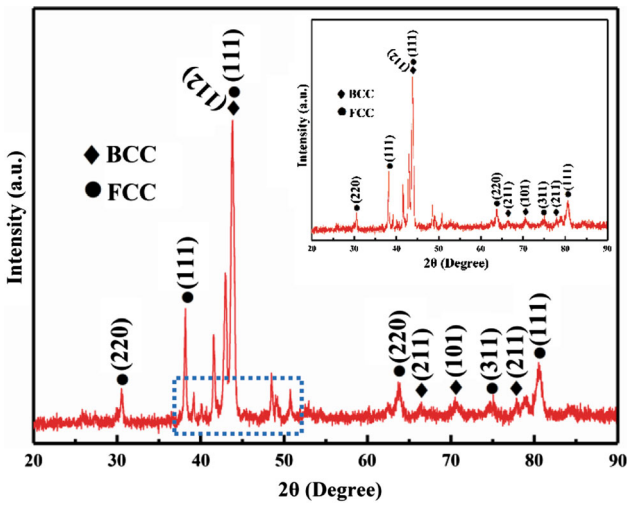

Fig. 2 XRD pattern of AlSiTiCrNiCu HEA

3. Results and Discussions

3.1 Microstructure Characterization

Figure 1(a)-(g) indicate the elemental distribution results of HEA by EPMA. It can be observed that the HEA is composed of white phase, gray phase and black phase, which are, respectively, marked as A, B and C. The A phase contains Al, Ti, Cu and Ni elements, and the elements constitute of B phase is same as A phase. The C phases consist of Si, Ti, Cr, Ni, and Cu elements. Meanwhile, the Cr element enriches in some areas of the black C phase. Figure 2 shows that the XRD diffraction pattern of AlSiTiCrNiCu HEA. The diffraction peaks are made up of body-centered cubic (BCC) phases and face-centered cubic (FCC) phases. The literature shows that there are two types of BCC1 and BCC2 structure. The BCC1 is the poor Cr phases, while the BCC2 phases should be Cr_3Si phases (Ref

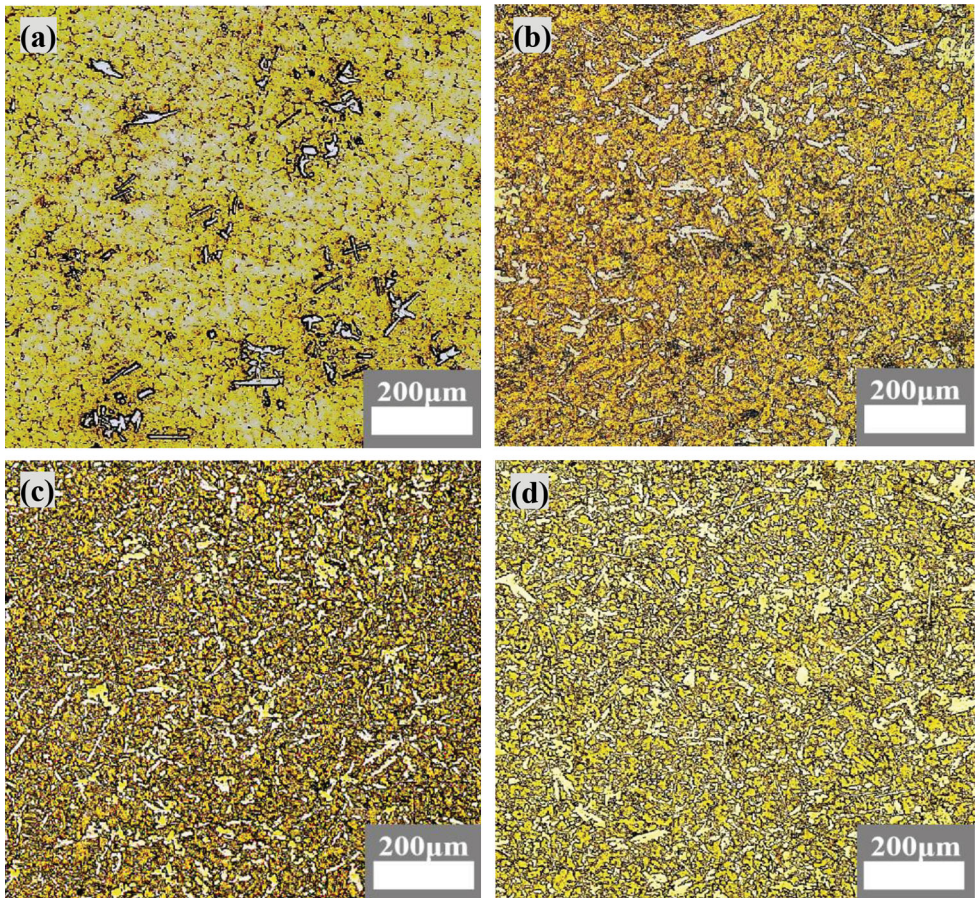

Fig. 3 Optical micrograph of pure Al with the various content of HEA: (a) 5.0 wt.% HEA; (b) 10.0 wt.% HEA; (c) 15.0 wt.% HEA; (d) 20.0 wt.% HEA

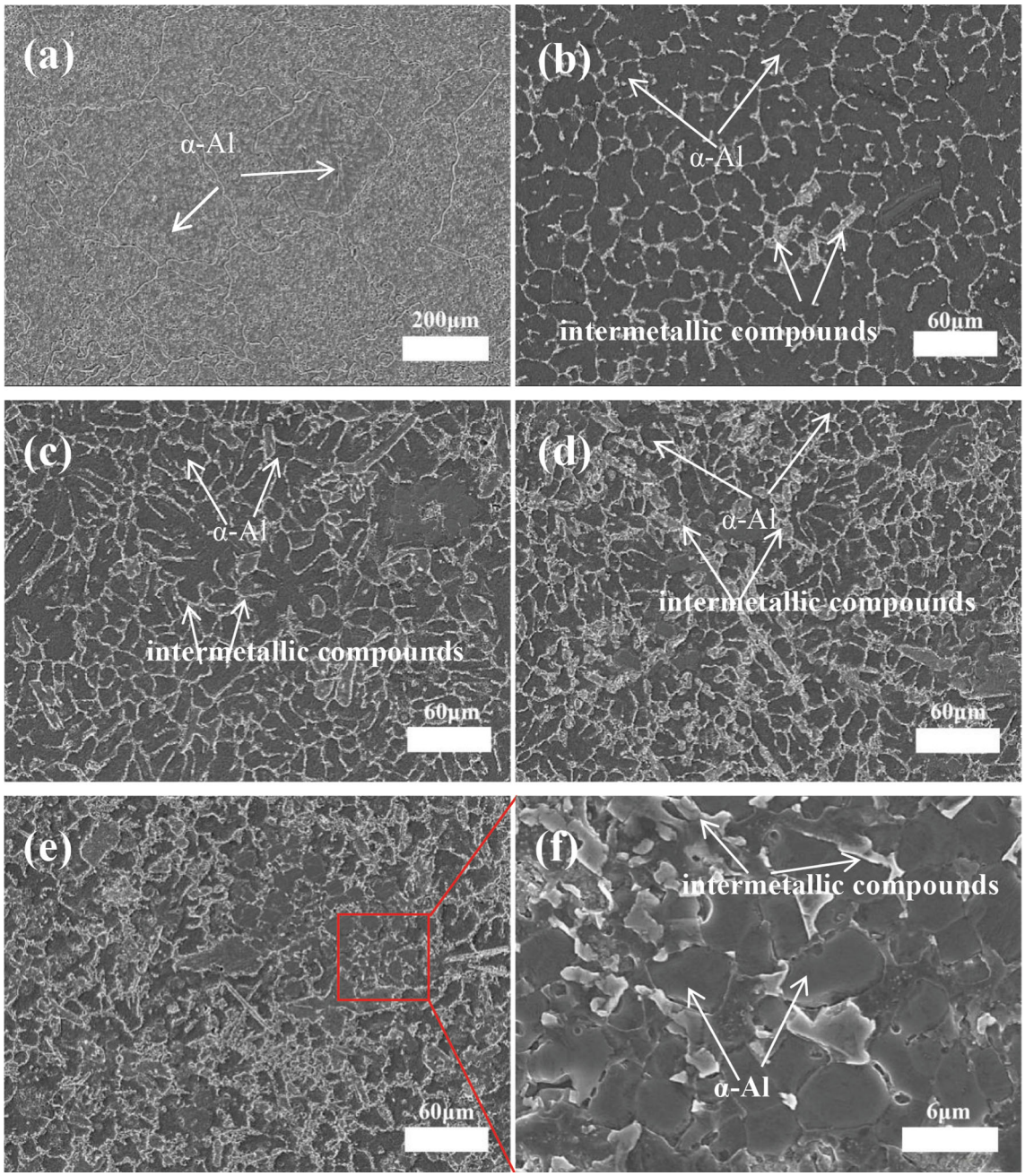

Fig. 4 SEM micrograph of pure Al with the different concentration of HEA: (a) without HEA; (b) 5.0 wt.% HEA; (c) 10.0 wt.% HEA; (d) 15.0 wt.% HEA; (e) 20.0 wt.% HEA; (f) magnified image of local area in (e)

29). In addition, the FCC should be the AlCuNi solid solution. On the basis of analysis results in Fig. 1 and 2, it can be concluded that three different phases are co-existence in HEA.

Figure 3 shows the optical micrograph of pure Al with various addition content of HEA. It is clearly shown from Fig. 3(a)-(d) that the microstructural morphology and precipitated intermetallic compounds present obvious change when the different content HEA (5.0, 10.0, 15.0 and 20.0 wt.%) are added to pure aluminum. The microstructure of AMCs with 5.0 wt.% HEA addition is demonstrated in Fig. 3(a). The irregular blocky and flake-like intermetallic compounds form and distribute in the α-Al matrix. After introducing 10.0 wt.% HEA, as shown in Fig. 3(b), the volume fraction of intermetallic compounds increase significantly. Hence, it is inferred that the amounts of intermetallic compounds increase with the increasing addition content of HEA, and their dimension also occurs to significant variation. Furthermore, the segregation phenomenon of the intermetallic compounds is remarkable. Sasikumar and Kumar (Ref 30) found that the segregation phenomenon is related to the motion velocity of the solid-liquid (S-L) interface during solidification. Figure 4 presents the micrograph of Al matrix composites with various adding concentration of HEA in pure Al. It also demonstrates the evolution process of α-Al dendrites. Figure 5 shows the average grains size of α-Al in Al matrix composites by adding different HEA content. Figure 4(a) shows the microstructure of pure Al, which consists of well-developed and irregular equiaxed crystal structure. In addition, the grain size of α-Al is about 220 μm.

Figure 4(b) is the microstructure of AMCs, which is prepared by introducing 5.0 wt.% HEA into pure Al. Compared with Fig. 4(a), the average grain size of the α-Al grains is sharply reduced to 41 μm. With the further increment of the adding content of HEA, it can be seen from Fig. 4(c) that the grain size of α-Al is obviously refined to 32 μm. When introducing content of HEA is up to 20.0 wt.%, the grain size of α-Al is decreased to 15 μm and the morphology obviously transforms from well-developed irregular equiaxed grains to dendritic structure, as shown in Fig. 4(e). It can be found from Fig. 5 that the size of α-Al decreases continuously with the increase of HEA addition content, and the size is the smallest when the addition content of HEA is 20.0 wt.%. This is due to the increase HEA addition concentration in pure Al, which leads to an increase in nucleation rate and the precipitated intermetallic compounds inhibits the growth of crystals (Ref 31). Lots of solute atoms are pushed to the front of solid-liquid interface in solidification due to very limited solid solubility, and multiple intermetallic compounds precipitate in the surface. Related research shows that the atoms aggregation on the interface can increase constitutional undercooling and restrict the crystal grows ahead of solid-liquid interface in solidification (Ref 32). Additionally, it is observed from Fig. 4(f) that the blocky intermetallic compounds are distributed in the grain boundaries. Figure 6 is high magnification SEM images of AMCs, which are prepared through adding different contents of HEA to pure Al. It can be distinctly revealed from Fig. 6(a) that white and discontinuous precipitates distribute in the grain boundary. When 10.0 wt.% HEA is introduced to pure Al preparing AMCs with multiple intermetallic compounds, the agglomeration phenomenon appears, as shown in Fig. 6(b). In addition, it can be evidently seen from Fig. 6(c) that the white precipitates

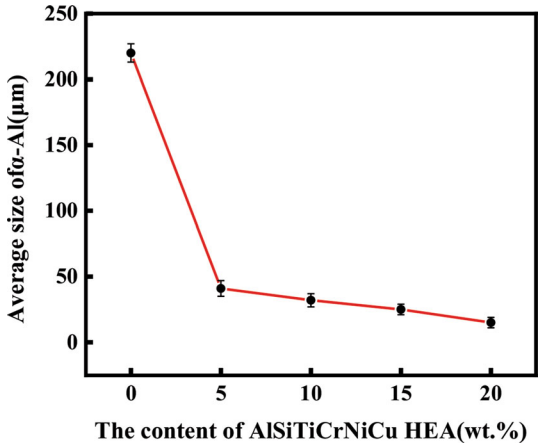

Fig. 5 The average size of α-Al in pure Al with the different HEA concentration

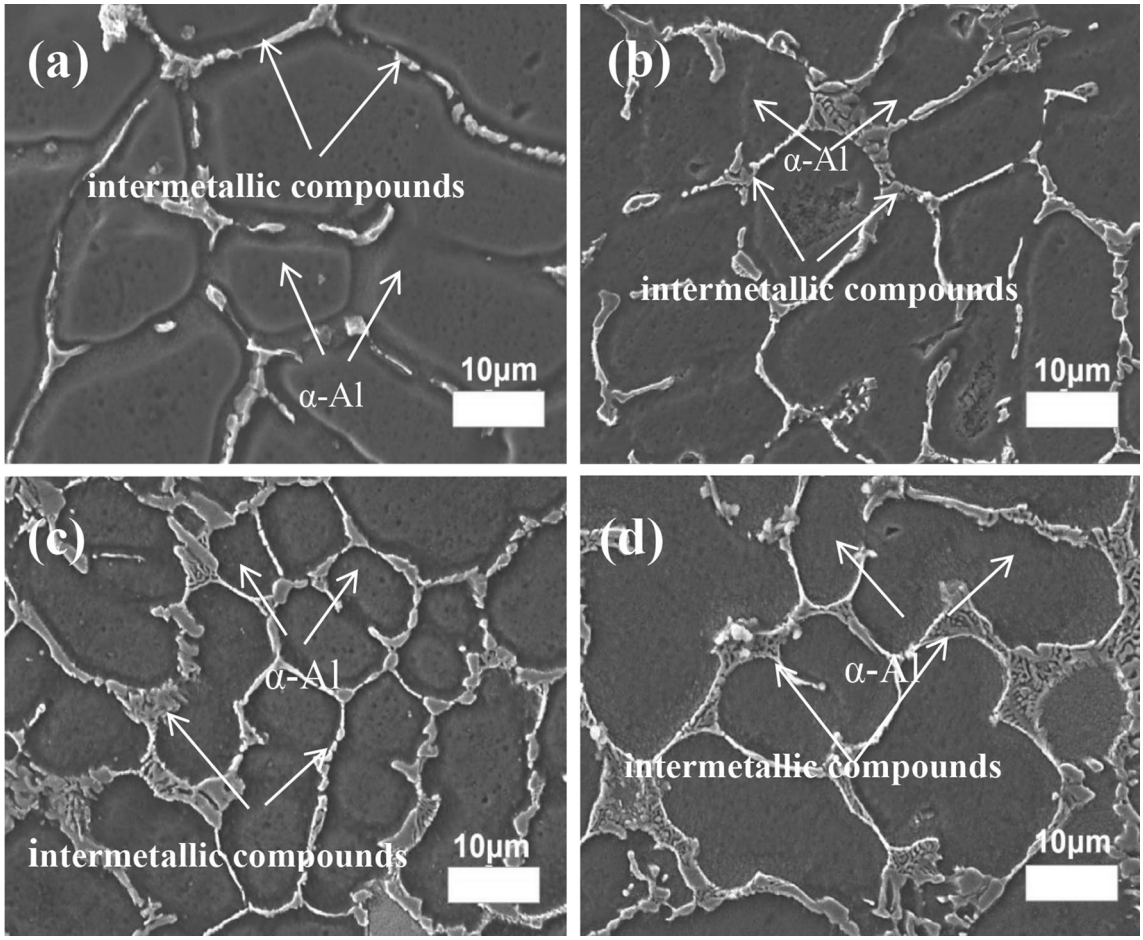

Fig. 6 High magnification SEM images of pure Al with the different content of HEA: (a) 5.0 wt.% HEA; (b) 10.0 wt.% HEA; (c) 15.0 wt.% HEA; (d) 20.0 wt.% HEA

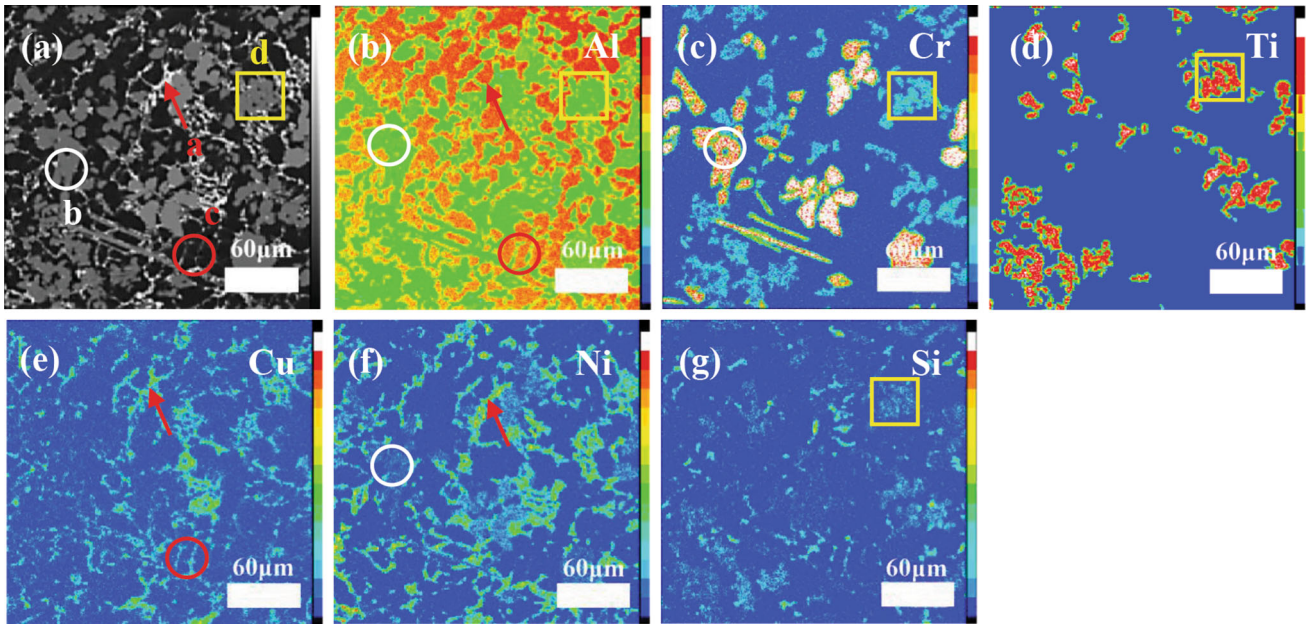

Fig. 7 EPMA analysis of AMCs with 20.0 wt.% HEA: (a) back-scattered electron image; (b) Al element; (c) Cr element; (d) Ti element; (e) Cu element; (f) Ni element; (g) Si element

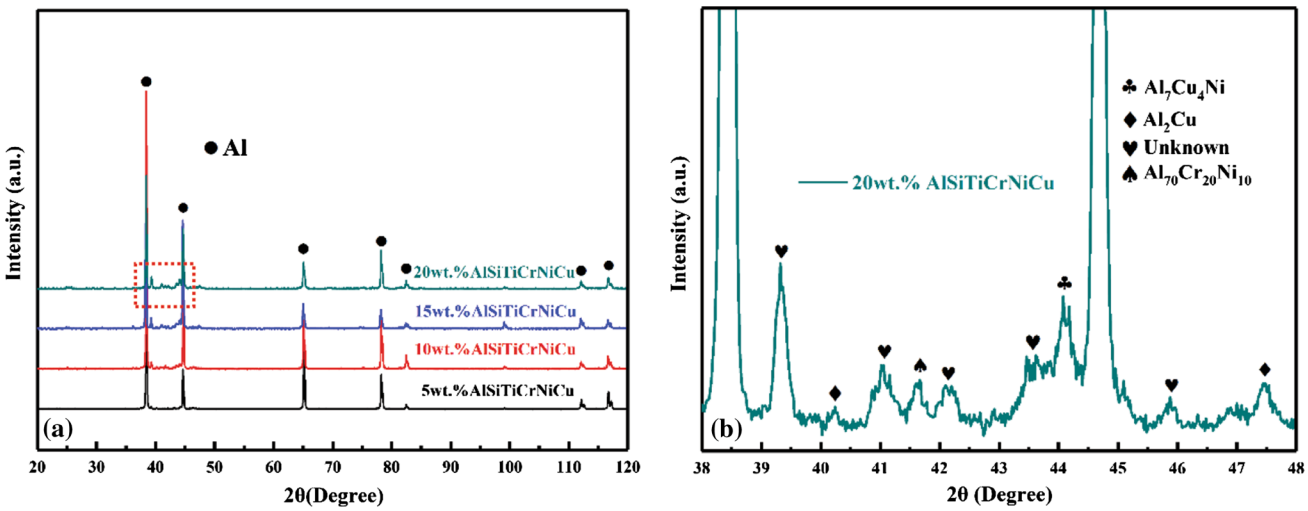

Fig. 8 (a) XRD patterns of pure Al with the different content of HEA addition; (b) magnified curves of local area in (a)

increase when the addition concentration of HEA increase to 15.0 wt.%. After the addition content of HEA further increases to 20.0 wt.%, the white precipitates continuously distribute and exist in the form of network structure, as shown in Fig. 6(d). Figure 7 exhibits the typical mapping analysis results of Al, Si, Ti, Cr, Ni and Cu elements in AMCs introducing 20.0 wt.% HEA. Obviously, the "a" is composed of Al, Cu and Ni elements (where the arrow points). The flake intermetallic compounds "b" consists of Al, Cr and Ni elements (indicated by the white circle). Moreover, the "c" contains Al and Cu elements (indicated by the yellow circle), and the blocky intermetallic compounds "d" is mainly composed of Al, Ti, Cr, and Si elements (indicated by the yellow box). Figure 8 presents the XRD pattern of AMCs. The various peaks (Al_2Cu, Al_7Cu_4Ni and $Al_{70}Cr_{20}Ni_{10}$) and unknown phases exist besides α-Al in the AMCs, as shown in Fig. 8. Combining Fig. 7 with Fig. 8, it can be inferred that the "a" phase is Al_7Cu_4Ni, and the "b" phase is $Al_{70}Cr_{20}Ni_{10}$. In addition, the "c" phase and "d" phase are Al_2Cu and AlTiCrSi, respectively.

3.2 Compression Properties

The compressive experiment is executed for the purpose of evaluating the compressive properties of AMCs. Figure 9 is the macroscopic photographs of the specimens after compression. Figure 9(a) demonstrates that pure Al has the excellent plasticity, and there is no visible crack on the surface of the compressive specimen. With the increase of the content of HEA, cracks are prematurely formed on the surface of compression specimen. Furthermore, AMCs also undergo a distinct ductile-brittle transition. Figure 9(b) is the compressive sample of AMCs reinforced by 15.0 wt.% HEA addition. It was found that the deformation initiates from the sample surface and develops into big cracks in a shear mode. Moreover, the cracks

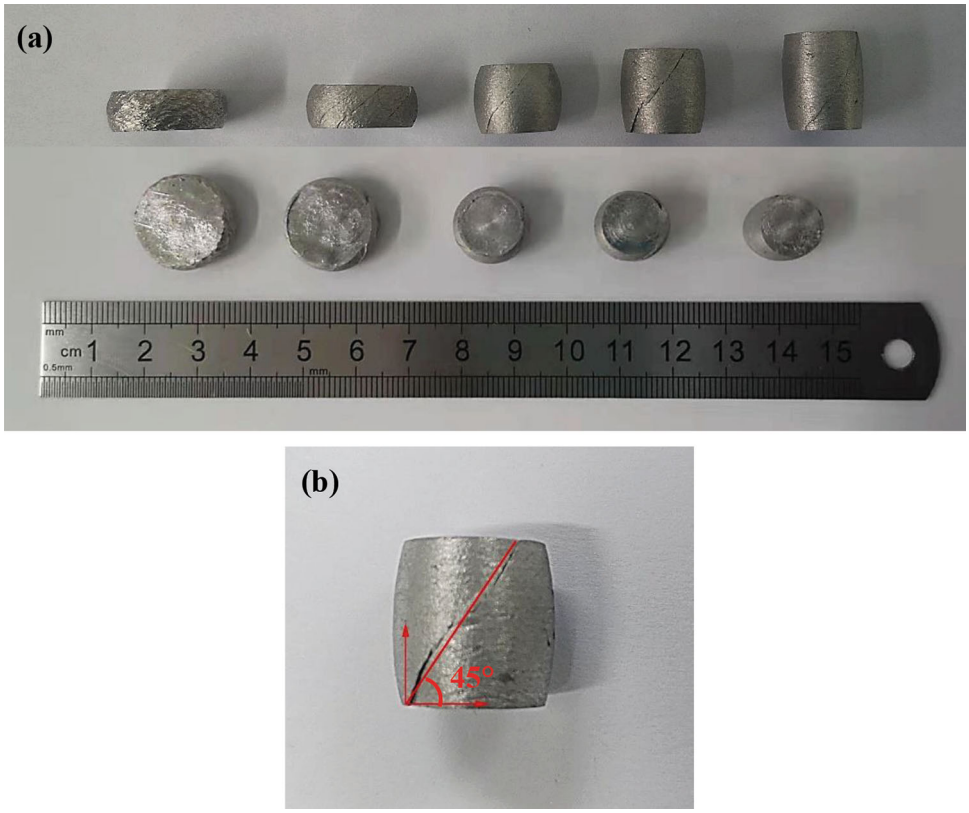

Fig. 9 Morphologies of as-cast compression specimens: (a) pure Al with various HEA addition (0, 5.0, 10.0, 15.0 and 20.0 wt.%); (b) AMCs adding 15.0 wt.% HEA

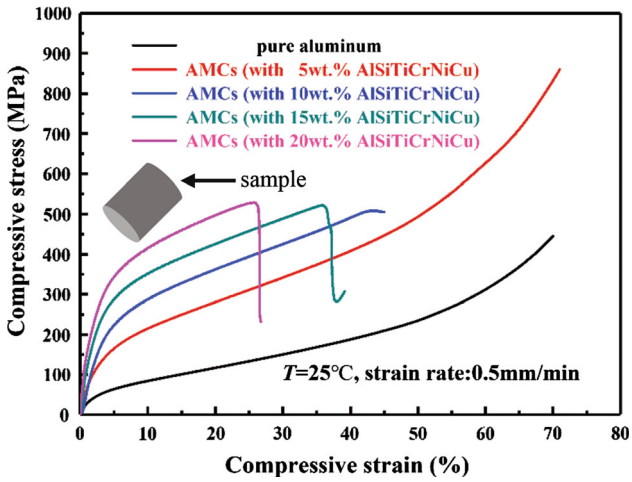

Fig. 10 The compressive stress-strain curves of pure Al adding different HEA addition

propagate in the direction of 45° with the loaded compression stress (Ref 33). Ye et al. (Ref 34) proposed that the most shear stress occurs to the direction of 45° between the loaded stress and the compressive sample. Therefore, all failure compression specimens have approximately identical shear fracture mode. Figure 10 indicates the compressive stress-strain curves of the AMCs. Table 2 presents the compressive properties of the pure Al and AMCs. The introduction of HEA results in significant improvement in the deformation resistance of pure Al. Hence, the compressive strength is positively correlated with the

Table 2 Compression properties of pure Al with various content HEA

HEA percentage	$\sigma_{0.2}$, MPa	Compressive strength, MPa	Strain, %
0 wt.%	45 ± 5	…	…
5.0 wt.%	128 ± 7	…	…
10.0 wt.%	214 ± 6	498	42.8
15.0 wt.%	276 ± 8	516	35.7
20.0 wt.%	318 ± 6	530	25.8

addition amount of HEA. Specifically, the yield strength of AMCs reinforced by 20.0 wt.% HEA addition is 318 ± 6 MPa, which is increased by 606.7% compared with the unreinforced pure Al (45 ± 5 MPa), and its compressive strength also is enhanced to 530 MPa. However, the plasticity of AMCs presents a negative relationship with the addition amount of HEA. It is worth notable that the transformation process of AMCs can be distinguished into two types: complete plasticity (5.0 wt.% HEA) and ductile-brittle transition (≥ 10.0 wt.% HEA). Particularly, the AMCs exhibit distinct breaking points and its compressive strain is more than 25% when the adding content of HEA is up to 20.0 wt.%. This is mainly attributed to the following two factors: (1) The presence of hard phases, such as Al_2Cu, Al_7Cu_4Ni, AlTiCrSi, and $Al_{70}Cr_{20}Ni_{10}$, which hinder the movement of dislocation (Ref 35). (2) The precipitated intermetallic compounds have high strength and hardness. The load applied to the substrate can be transferred to the reinforcing phase during the deformation process (Ref 22-

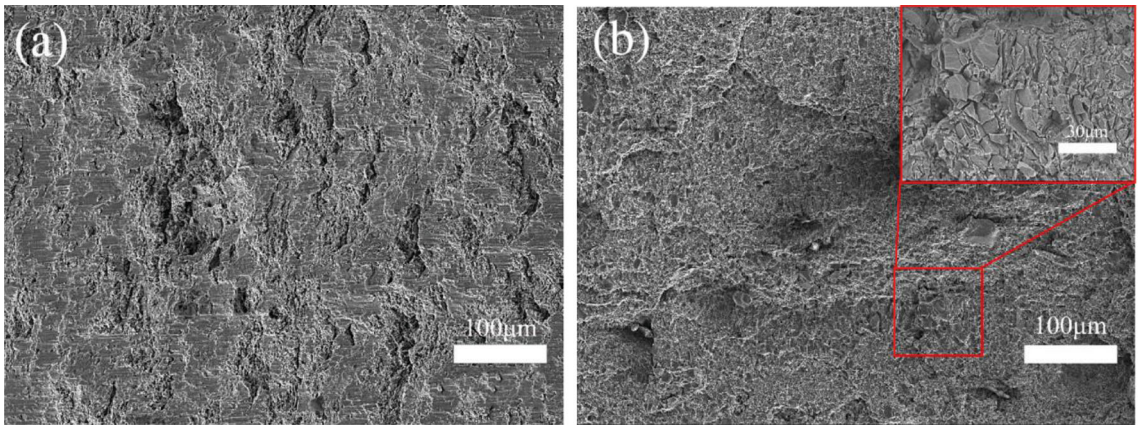

Fig. 11 The compressive fracture surfaces of AMCs: (a) 15.0 wt.% HEA; (b) 20.0 wt.% HEA

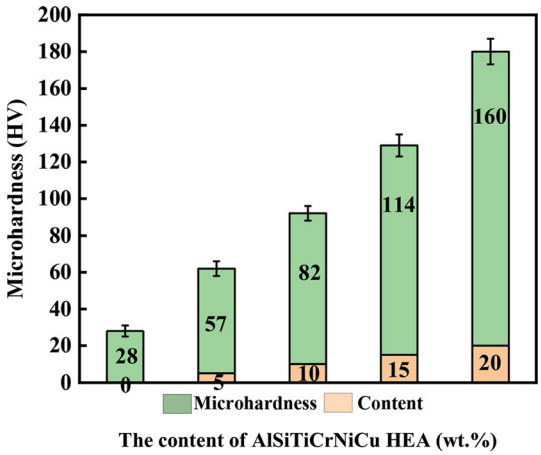

Fig. 12 The microhardness of pure Al with different HEA content

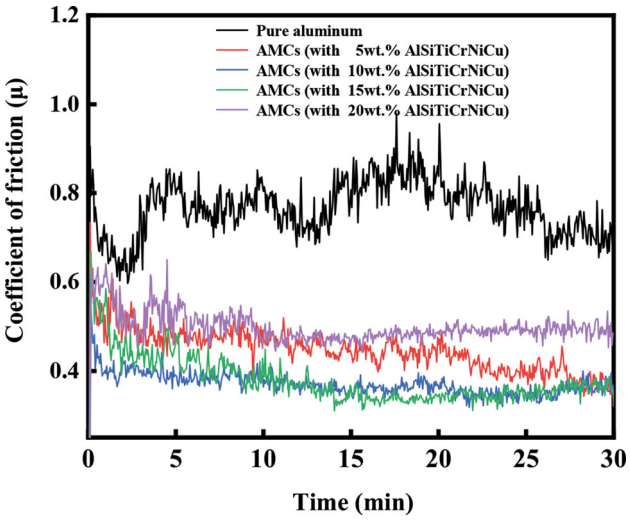

Fig. 13 The change in COF curves of pure Al adding different HEA content

24). It has been reported that the contribution of load transfer on strength during the mechanical test can be calculated based on the improving shear lag theory model. The expression is given by reference (Ref 36):

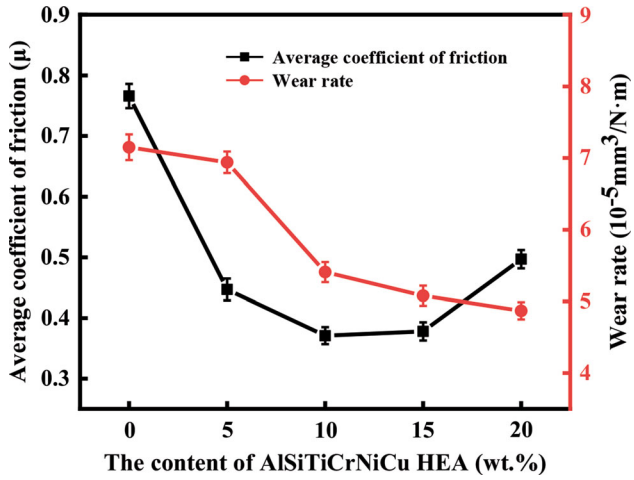

Fig. 14 Average COF and wear rate of pure Al with various HEA content

$$\Delta\sigma_{\text{load}} = 0.5 V_P \sigma_m \quad \text{(Eq 1)}$$

where, σ_m is the yield strength of pure Al and V_P is the volume fraction of the reinforcements. Equation 1 demonstrates that $\Delta\sigma_{\text{load}}$ is a linear relationship with V_P. The V_P change will inevitably lead to change in strength. Meanwhile, according to the Hall-Petch formula (Ref 37):

$$\Delta\sigma = k\left(d^{-\frac{1}{2}} - d_0^{-\frac{1}{2}}\right) \quad \text{(Eq 2)}$$

where k is Hall-Petch coefficient; d are mean grain diameter. Following the formula (2), the improvement in the strength of AMCs is due to the reduction of grain diameter. In addition, the compression fracture morphology of the composites is shown in Fig. 11. The fracture surface of the AMCs reinforced by 15.0 wt.% HEA addition is composed of many slip bands, and its fracture feature is dominated by the slip fracture, whereas the fracture surface of AMCs exhibits typical ductile-brittle mixed fracture when the addition content of HEA is up to 20.0 wt.%.

3.3 Microhardness

According to the previous research on the microstructure of AMCs, the HEA is introduced into pure Al preparing aluminum matrix composites reinforced by multiphase intermetallic

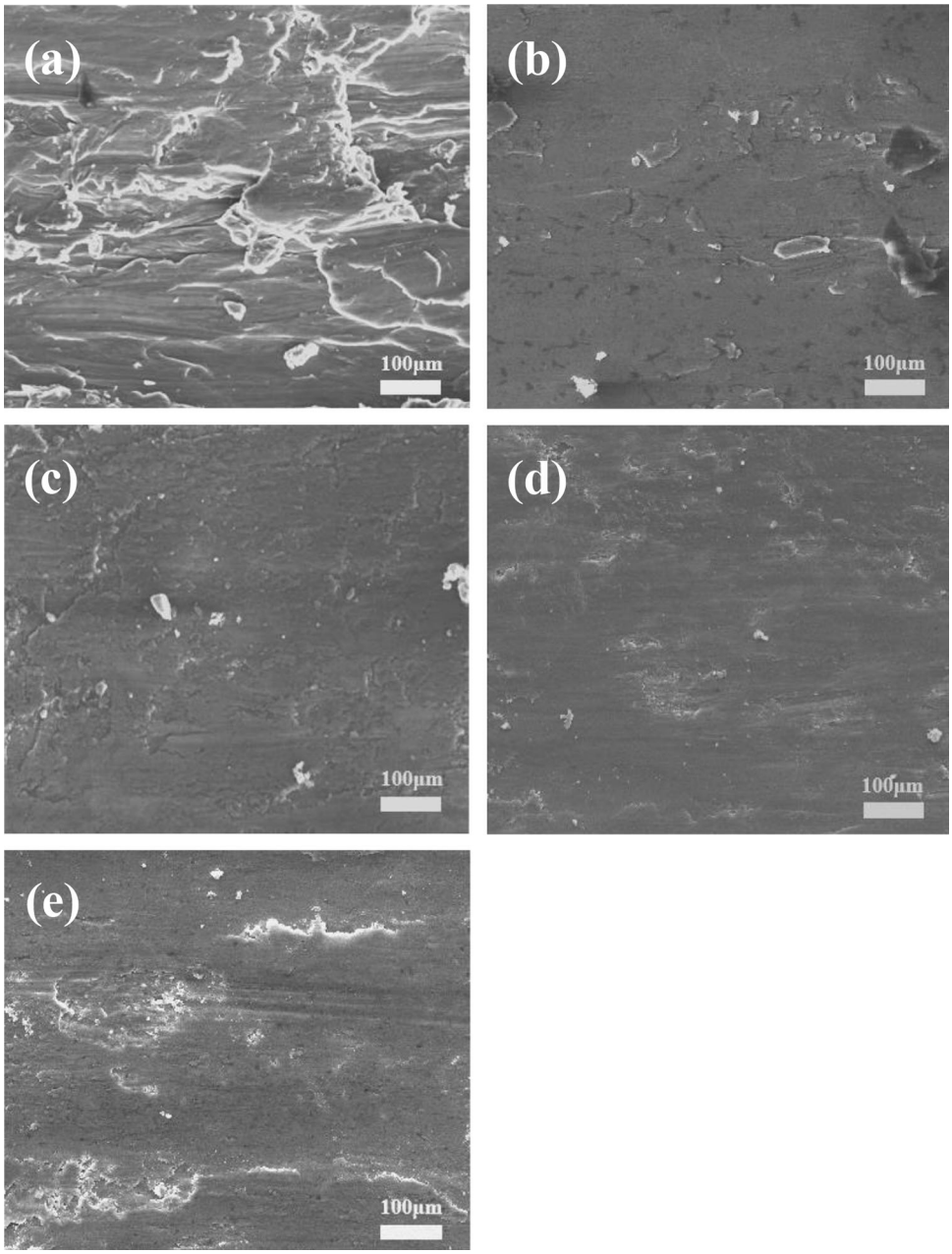

Fig. 15 Low magnification SEM micrographs of worn surfaces of pure Al with different HEA contents: (a) without HEA; (b) 5.0 wt.% HEA; (c) 10.0 wt.% HEA; (d) 15.0 wt.% HEA; (e) 20.0 wt.% HEA

compounds (Ref 27). Thus, the measurement of microhardness is crucial to evaluate the reinforcement effect. In order to ensure the accuracy of microhardness values measured by the experiment, five different positions are selected for microhardness test on each specimen, and the Vickers hardness of pure Al and AMCs with different content of HEA addition is reflected in Fig. 12. It is found that the microhardness value of the AMCs significantly increase with the volume fraction of the reinforcement of multiple intermetallic compounds. This is because that the fraction of hard and brittle intermetallic compounds also increases as the adding content of HEA increases, which improve the microhardness of AMCs. Specifically, the microhardness value of pure Al is only 28 HV, which is lower than the microhardness value (57 HV) of the AMCs reinforce by 5.0 wt.% HEA addition. When 10 and 15 wt.% HEA is introduced to pure Al preparing AMCs, the microhardness improves to 82 HV and 114 HV, respectively. Moreover, the microhardness value of the AMCs reinforced by 20.0 wt.% HEA addition is up to 160 HV. Generally, the AMCs with outstanding microhardness usually will present superior wear-resistance performance based on the numerous previous research results, such as the AMCs reinforced by B_4C, TiB_2 reinforcement (Ref 38, 39). Therefore, it is necessary to study the sliding friction behavior of AMCs reinforced by adding HEA to pure Al.

3.4 Friction Properties

Figure 13 reveals the dry sliding coefficient of friction (COF) curve for the pure Al and AMCs under the same conditions (10 N and 200 r/s). Distinctly, compared with pure

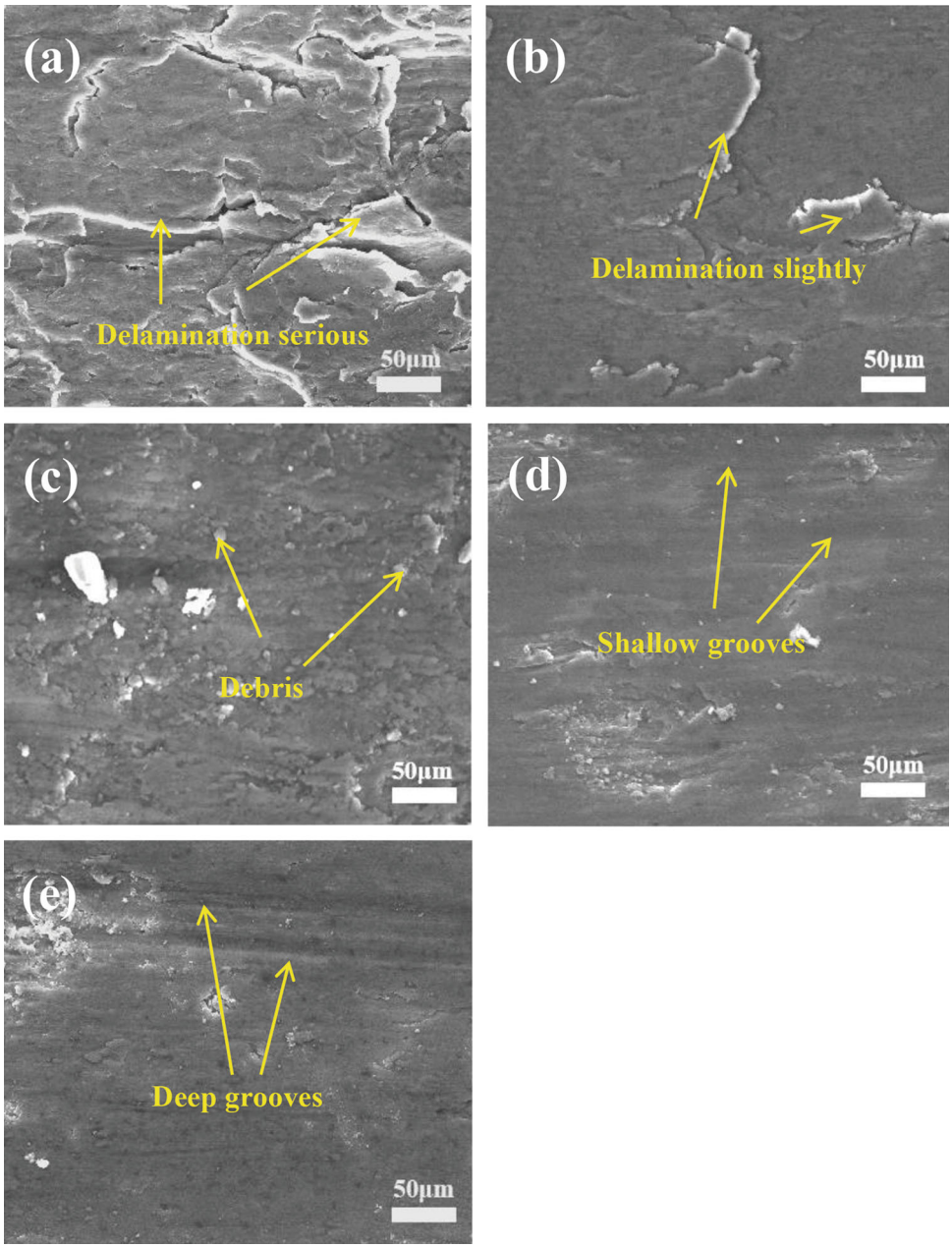

Fig. 16 High magnification SEM micrographs of worn surfaces of pure Al with different HEA contents: (a) without HEA; (b) 5.0 wt.% HEA; (c) 10.0 wt.% HEA; (d) 15.0 wt.% HEA; (e) 20.0 wt.% HEA

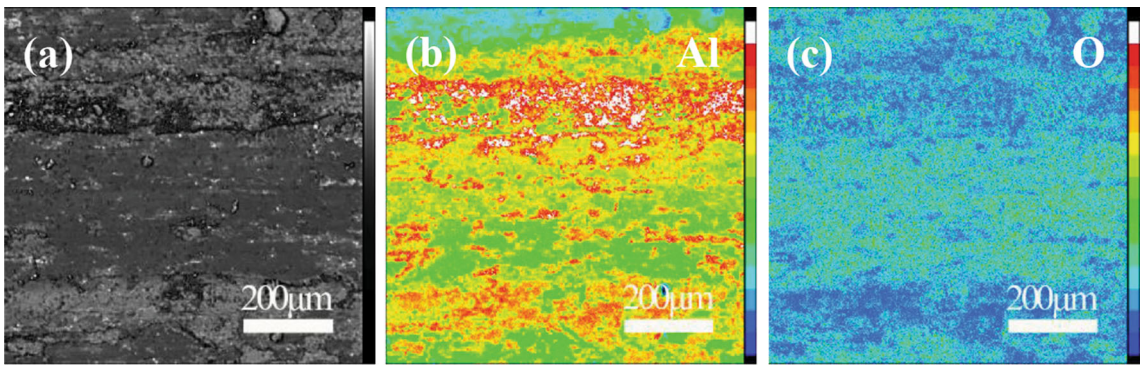

Fig. 17 EPMA analysis of worn surfaces of pure Al: (a) back-scattered electron image; (b) Al element; (c) O element

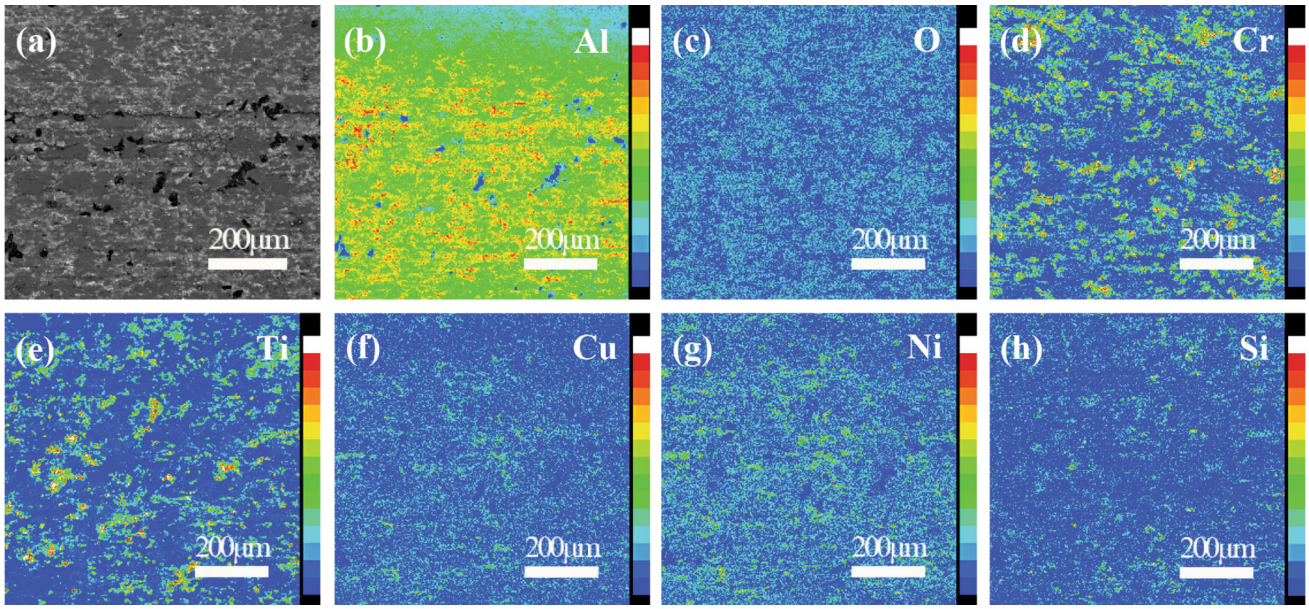

Fig. 18 EPMA analysis of worn surfaces of AMCs with 20.0 wt.% HEA: (a) back-scattered electron image; (b) Al element; (c) O element; (d) Cr element; (e) Ti element; (f) Cu element; (g) Ni element; (h) Si element

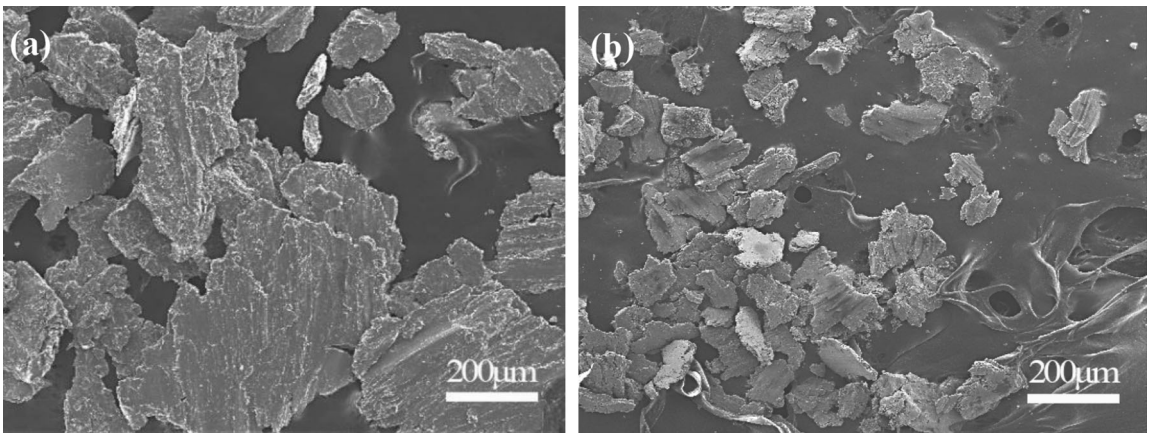

Fig. 19 SEM images of worn debris: (a) pure Al; (b) AMCs with 20.0 wt.% HEA

Al, the COF of AMCs is lower and the fluctuation amplitudes is small. It is observed from the curve of COF that pure Al exhibits the highest fluctuation amplitudes. This is because that a large quantity of debris and residual caters are formed on the worn surface during severe wear processes (Ref 7). In addition, Adegbenjo et al. (Ref 40) found that the large fluctuation amplitudes of COF are affected by the adhesive wear mechanism of pure Al. However, the composites exhibit higher mechanical properties and its surface oxide film is not easily damaged during the friction process, which results in lower fluctuation amplitude of the COF (Ref 7). In addition, Fig. 14 intuitively reflects the average COF and wear rate of pure Al and AMCs. The COF of pure Al is as extremely high as 0.766, and the wear rate is 7.15×10^{-5} mm^3/N·m. This is related to some characteristics of pure Al, such as low strength, low hardness and low plastic deformation resistance. It also can be seen from Fig. 14 that the COF and wear rate of the AMCs significantly decrease with the increase of the content of HEA addition. When the addition amount of HEA reaches 10.0 wt.%, the COF of AMCs is only 0.371. Compared with the pure Al, the COF of ACMs is reduced by 51.6%. However, with the further increase of the HEA content addition, the COF of the ACMs begins to increase. The wear rate of the ACMs continues to decrease with the increase of the HEA content. When the HEA adding content is 20.0 wt.%, the wear rate reaches the minimum of 4.87×10^{-5} mm^3/N·m, which is reduced by 31.9% compared with pure Al. Zhang et al. (Ref 41) conducted scratch and wear tests on SiC and Al_2O_3 particle-reinforce 6061 ACMs and found that the COF of the material was improved with the increase of particles addition content. The Rohatgi et al. (Ref 42) showed that the COF of the composites was reduced when solid lubricating particles such as graphite were added to the Cu matrix. However, when the graphite content exceeds 20.0 wt.%, the COF of the copper-based composites occurred to increasing. In this study, with the increase of HEA addition, the volume fraction of forming hard and brittle intermetallic compounds in solidification increase distributed in matrix leading to hardness improving of AMCs. Therefore, when the adding content of HEA reaches 15.0 wt.%, the COF of ACMs begins to increase. However, these

precipitating intermetallic compounds distributing in soft α-Al matrix can decrease the direct contact between the friction medium and Al matrix. Hence, the wear rate of the ACMs occurs to reduce with the increase of forming intermetallic compounds in solidification. Figure 15 and 16 exhibits the SEM images of the worn surface of pure Al and AMCs at different magnifications. The wear surface of pure Al has an obvious delamination, severe plastic deformation, and violent adhesive wear activities, as shown in Fig. 15(a). Moreover, in the process of friction and wear, it is observed that the surface of pure Al sample happens to peel off, as shown in Fig. 16(a). Hence, the wear mechanism of pure Al should be delamination wear and adhesive wear (Ref 7). It is found in Fig. 15(b) and 16(b) that the delamination and adhesive wear phenomenon on the worn surface is significantly weakened than that of pure Al sample when the addition amount of HEA is 5.0 wt.%. In addition, it is observed from Fig. 15(c) and (d) that the delamination of the worn surface is further reduced and accompanied by slight adhesive wear when 10.0 and 15.0 wt.% HEA is introduced to pure Al. Moreover, the shallow grooves and some debris can be observed at corresponding high magnification, as shown in Fig. 16(c) and (d). When the increment of HEA is up to 20.0 wt.%, the surface appears severe abrasive wear accompanied by deep grooves, as demonstrated in Fig. 15 (e) and Fig. 16(e). The previous studies have illustrated that composites easily formed mechanical mixed layer (MML) on the wear surface, which is constituted of reinforcing phase, matrix and oxides. Moreover, the hard MML will reduce the loss of material during friction process (Ref 43, 44). Meanwhile, the forming debris exists in the friction surface and acts as MML (Ref 43). In addition, the steel ball and the matrix can be isolated by forming the MML, which can act as solid lubricant decreasing the COF (Ref 45).

Figure 17 and 18 shows EPMA analysis results of worn surface of pure Al and AMCs with 20.0 wt.% HEA addition, respectively. It is worth noticing that the oxygen content of the former is significantly higher than the latter. This result indicates that the pure Al is more prone to oxidation during dry sliding friction. The content of Al and O elements are particularly high on the friction surface of pure Al. Therefore, the worn surface of pure Al is mainly dominated by oxides. Moreover, the MML layer is relatively sparse and thin. Although the oxygen content slightly decreases with the increase of reinforcement, the content of Cr, Ti, Cu, and Si elements distinctly improve, as shown in Fig. 18. The MML with abundant intermetallic compounds and oxides can be clearly observed on the friction surface of preparing AMCs with 20.0 wt.% HEA addition.

Figure 19 presents SEM images of worn debris collected from pure Al and AMCs with 20.0 wt.% HEA addition to further investigate their tribological behavior. Figure 19(a) reveals the worn debris of pure Al. It can be observed from Fig. 19(a) that the debris exists in the form of large flakes, which indicates typical delamination wear mechanism. Compared with pure Al, the size of worn debris of the AMCs reinforced by 20.0 wt.% HEA addition is significantly reduced, and there are also some small particles, as shown in Fig. 19(b). The phenomenon shows that the wear mechanism of the AMCs is abrasive wear (Ref 7). Combined with the above analysis, it can be inferred that as the content of HEA increases, the volume fraction of hard and brittle compounds in the matrix increases. The reinforcing phases also act as MML and protect the friction surface. Therefore, the wear rate of AMCs gradually decreases and the wear mechanism transfers from layered and abrasive wear in pure Al to abrasive wear in AMCs.

4. Conclusions

In this study, a novel aluminum matrix composites reinforced by multiphase intermetallic compounds were fabricated through conventional casting approach. Conclusions from this work are as follows:

1. The fraction of precipitated multiphase intermetallic compounds gradually increases with the increase of HEA addition, and the grain size of α-Al obviously reduces.
2. The irregular multiphase intermetallic compounds, such as Al70Cr20Ni10 and AlTiCrSi, are distributed in the Al matrix; however, the Al_2Cu and Al_7Cu_4Ni are distributed in inter-dendrites of α-Al.
3. The compression strength of AMCs reinforced by 20.0 wt.% HEA is enhanced to 530 MPa due to the precipitation of multiphase intermetallic compounds. Meanwhile, its compression strain exceeds 25%.
4. Compared with pure Al, the microhardness of AMCs is extremely increased to 160 HV when the addition content of HEA is up to 20.0 wt.%. When the addition amount of HEA reaches 10.0 wt.% that the COF of the ACMs is decreased by 51.6% from 0.766 to 0.371. When the HEA content is 20.0 wt.%, the wear rate reaches the minimum of 4.87×10^{-5} $mm^3/N{\cdot}m$, which is reduced by 31.9% compared with pure Al. Judging from the friction surface, the wear mechanism of pure Al is layered wear and abrasive wear, but the ACMs prepared by adding 20 wt.% HEA is abrasive wear.

Acknowledgments

This work financially supports of the National Natural Science Foundation of China (Grant Nos. 52061026; 51561021), the State Key Laboratory of Advanced Processing and Recycling of Nonferrous Metals, Lanzhou University of Technology (SKLAB02019007), Key Research and Development Program of Gansu Province (21YF5GA075) and Outstanding Graduate Student "Innovation Star" Project of Gansu (2021CXZX-428, 2021CXZX-435).

References

1. C. Suryanarayana, and Nasser Al-Aqeeli, Mechanically Alloyed Nanocomposites, *Prog. Mater. Sci.*, 2013, **58**, p 383–502
2. J.W. Zhu, W.M. Jiang, G.Y. Li, F. Guan, Y. Yu, and Z.T. Fan, Microstructure and Mechanical Properties of SiCp/Al6082 Aluminum Matrix Composites Prepared By Squeeze Casting Combined With Stir Casting, *J. Mater. Process. Technol.*, 2020, **283**, p 116699
3. W.M. Jiang, J.W. Zhu, G.Y. Li, F. Guan, Y. Yu, and Z.T. Fan, Enhanced Mechanical Properties of 6082 Aluminum Alloy Via SiC Addition Combined with Squeeze Casting, *J. Mater. Sci. Technol.*, 2021, **188**, p 119–131
4. Y. Tang, Z. Chen, A. Borbely, G. Ji, S.Y. Zhong, D. Schryvers, V. Ji, and H.W. Wang, Quantitative Study of Particle Size Distribution in an in-Situ Grown Al-TiB_2 Composite by Synchrotron X-Ray Diffraction and Electron Microscopy, *Mater. Char.*, 2015, **102**, p 131–136

5. Y. Yang, S.F. Wen, Q.S. Wei, W. Li, J. Liu, and Y.S. Shi, Effect of Scanline Spacing on Texture, Phase and Nano Hardness of TiAl/TiB_2 Metal Matrix Composites Fabricated by Selective Laser Melting, *J. Alloy. Compd.*, 2017, **728**, p 803–814
6. F. Ali, S. Scudino, M.S. Anwar, R.N. Shahid, V.C. Srivastava, V. Uhlenwinkel, M. Stoica, G. Vaughan, and J. Eckert, Al-Based Metal Matrix Composites Reinforced with Al-Cu-Fe Quasi Crystalline Particles: Strengthening by Interfacial Reaction, *J. Alloy. Compd.*, 2014, **607**, p 274–279
7. C.X. Zhang, D.X. Yao, J.W. Yin, K.H. Zuo, Y.F. Xia, and H.Q. Liang, Effects of β-Si_3N_4 Whiskers Addition on Mechanical Properties and Tribological Behaviors of Al Matrix Composites, *Wear*, 2019, **430–431**, p 145–156
8. J.J. Zhang, S.C. Liu, Y.P. Lu, Y. Dong, and T.J. Li, Fabrication Process and Bending Properties of Carbon Fibers Reinforced Al-Alloy Matrix Composites, *J. Mater. Process. Technol.*, 2016, **231**, p 366–373
9. C.R. Si, X.L. Tang, X.J. Zhang, J.B. Wang, and W. Wu, Microstructure and Mechanical Properties of Particle Reinforced Metal Matrix Composites Prepared by Gas-Solid Two-Phase Atomization and Deposition Technology, *Mater. Lett.*, 2017, **201**, p 78–81
10. S.F. Li, K. Kondoh, H. Imai, B. Chen, L. Jia, J. Umeda, and Y. Fu, Strengthening Behavior of In Situ-Synthesized (TiC-TiB)/Ti Composites by Powder Metallurgy and Hot Extrusion, *Mater. Des.*, 2016, **95**, p 127–132
11. G.Y. Li, W.M. Jiang, F. Guan, J.W. Zhu, Z. Zhang, and Z.T. Fan, Microstructure Mechanical Properties and Corrosion Resistance of A356 Aluminum/AZ91D Magnesium Bimetal Prepared by a Compound Casting Combined with a Novel Ni-Cu Composite Interlayer, *J. Mater. Process. Tech.*, 2021, **288**, p 116874
12. X.L. Guo, Q. Guo, J.H. Nie, Z.Y. Liu, Z.Q. Li, G.L. Fan, D.B. Xiong, Y.S. Su, J.Z. Fan, and D. Zhang, Particle Size Effect on the Interfacial Properties of SiC Particle-Reinforced Al-Cu-Mg Composites, *Mater. Sci. Eng. A*, 2018, **711**, p 643–649
13. S.C. Tjong, Novel Nanoparticle-Reinforced Metal Matrix Composites with Enhanced Mechanical Properties, *Adv. Eng. Mater.*, 2007, **9**, p 639–652
14. J.W. Yeh, S.K. Chen, S.J. Lin, J.Y. Gan, T.S. Chin, and T.T. Shun, Nanostructured High-Entropy Alloys with Multiple Principal Elements: Novel Alloy Design Concepts and Outcomes, *Adv. Eng. Mater.*, 2004, **6**, p 299–303
15. A. Erdogan, A. Gunen, M.S. Gok, and S. Zeytin, Microstructure and Mechanical Properties of Borided CoCrFeNiAl0.25Ti0.5 High Entropy Alloy Produced by Powder Metallurgy, *Vacuum*, 2020, **183**, p 109820
16. G. Laplanche, P. Gadaud, O. Horst, F. Otto, G. Eggeler, and E.P. George, Temperature Dependencies of the Elastic Moduli and Thermal Expansion Coefficient of an Equiatomic, Single-Phase CoCrFeMnNi High-Entropy Alloy, *J. Alloy. Comp.*, 2015, **623**, p 348–353
17. K. Praveen-Kumar, M. Gopi-Krishna, J. Babu-Rao, and N.R.M.R. Bhargava, Fabrication and Characterization of 2024 Aluminum-High Entropy Alloy Composites, *J. Alloy. Comp.*, 2015, **640**, p 421–427
18. I. Carcea, R. Chelariu, L. Asavei, N. Cimpoeşu, and R.M. Florea, Investigations on Composites Reinforced with HEA Particles, *Mater. Sci. Eng. A*, 2017, **227**, p 012021
19. Z.W. Yuan, W.B. Tian, F.G. Li, Q.Q. Fu, Y.B. Hu, and X.G. Wang, Microstructure and Properties of High-Entropy Alloy Reinforced Aluminum Matrix Composites by Spark Plasma Sintering, *J. Alloy. Comp.*, 2019, **806**, p 901–908
20. Z.W. Wang, Y.B. Yuan, R.X. Zheng, K. Ameyama, and C.L. Ma, Microstructures and Mechanical Properties Extruded 2024 Aluminum Alloy Reinforced by FeNiCrCoAl$_3$ Particles, *Trans. Nonferrous Met. Soc. China.*, 2014, **24**(7), p 2366–2373
21. M.Q. Luo, D.Z. Zhu, L.F. Qi, Q. Chen, and L.J. Li, Properties of Al_xCuFeNiCo (Cr) High Entropy Alloys Particles Reinforced Aluminum Alloy Materials, *South. Met.*, 2016, **6**, p 18–22
22 G.M. Karthik, S. Panikar, G.D. Janaki-Ram, and R.S. Kottada, Additive Manufacturing of an Aluminum Matrix Composite Reinforced with Nanocrystalline High-Entropy Alloy Particles, *Mater. Sci. Eng. A*, 2016, **679**, p 193–203
23. Z. Tan, L. Wang, Y.F. Xue, P. Zhang, T.Q. Cao, and X.W. Cheng, High-entropy Alloy Particle Reinforced Al-Based Amorphous Alloy Composite with Ultrahigh Strength Prepared by Spark Plasma Sintering, *Mater. Des.*, 2016, **109**, p 219–226
24. J. Chen, P.Y. Niu, T. Wei, L. Hao, Y.Z. Liu, X.H. Wang, and Y.L. Peng, Fabrication and Mechanical Properties of AlCoNiCrFe High-Entropy Alloy Particle Reinforced Cu Matrix Composites, *J. Alloy. Comp.*, 2015, **649**, p 630–634
25. M. Balakrishnan, I. Dinaharan, K. Kalaiselven, and R. Palanivel, Friction Stir Processing of Al_3Ni Intermetallic Particulate Reinforced Cast Aluminum Matrix Composites: Microstructure and Tensile Properties, *J. Mater. Res. Technol.*, 2020, **9**, p 4356–4367
26. S.M. Ma, Y.S. Wang, and X.M. Wang, The In-Situ Formation of Al_3Ti Reinforcing Particulates in an Al-7wt%Si Alloy and their Effects on Mechanical Properties, *J. Alloy. Comp.*, 2019, **792**, p 365–374
27. Q.L. Li, X.P. Bao, S. Zhao, Y.Q. Zhu, Y.F. Lan, X.Y. Feng, and Q. Zhang, The Influence of AlFeNiCrCoTi High-Entropy Alloy on Microstructure, Mechanical Properties and Tribological Behaviors of Aluminum Matrix Composites, *Int. J. Metal. Cast.*, 2020 https://doi.org/10.1007/s40962-020-00462-x
28. J.H. Pi, Y.P.L. Zhang, and H. Zhang, Microstructure and Property of AlTiCrFeNiCu High-Entropy Alloy, *J. Alloy. Compd.*, 2011, **509**, p 5641–5645
29. D. Zhu, L. Qi, and X. Ding, Effect of Reinforcement Volume Fraction and Sintering Temperature on Thermal Conductivity of (AlSiTiCrNi-Cu)p/6061Al Composites, *Rare. Metal. Mat. Eng.*, 2019, **48**, p 614–619
30. R. Sasikumar, and M. Kumar, Redistribution of Particles During Casting of Composite Melts: Effects of Buoyancy and Particle Pushing, *Acta Metall. Mater.*, 1991, **39**, p 2503–2508
31. Y. Zhao, S. Zhang, G. Chen, and X. Cheng, Effects of Molten Temperature on the Morphologies of In Situ Al_3Zr and ZrB_2 Particles and Wear Properties of (Al_3Zr+ ZrB_2)/Al Composites, *Mater. Sci. Eng. A*, 2007, **457**, p 156–161
32. T.J. Chen, R.Q. Wang, and Y. Ma, Grain Refinement of AZ91D Magnesium Alloy by Al-Ti-B Master Alloy and its Effect on Mechanical Properties, *Mater. Des.*, 2012, **34**, p 637–648
33. M. ChulJo, J.H. Choi, J. Yoo, D. Lee, S. Shin, I. Jo, and S.K. Lee, Novel Dynamic Compressive and Ballistic Properties in 7075–T6 Al-matrix Hybrid Composite Reinforced with SiC and B4C Particulates, *Compos. Part B.*, 2019, **174**, p 107041
34. T.K. Ye, Y.X. Xu, and J. Ren, Effects of SiC Particle Size on Mechanical Properties of SiC Particle Reinforced Aluminum Metal Matrix Composite, *Mater. Sci. Eng. A*, 2019, **753**, p 146–155
35. S.F. Liu, Y.W. Wang, T. Muthuramalingam, and G. Anbuchezhiyan, Effect of B_4C and MoS_2 Reinforcement on Micro Structure and Wear Properties of Aluminum Hybrid Composite for Automotive Applications, *Compos. Part B.*, 2019, **176**, p 107329
36. Q.C. Fan, B.S. Li, and Y. Zhang, The Microstructure and Properties of (FeCrNiCo)Al_xCu_y High-Entropy Alloys and their TiC-Reinforced Composites, *Mater. Sci. Eng. A*, 2014, **598**, p 244–250
37. X. Zhang, L.K. Huang, B. Zhang, Y.Z. Chen, and F. Liu, Microstructural Evolution and Strengthening Mechanism of an Al-Si-Mg Alloy Processed by High-Pressure Torsion with Different Heat Treatments, *Mater. Sci. Eng. A*, 2020, **794**, p 139932
38. L. Yuan, J. Han, J. Liu, and Z. Jiang, Mechanical Properties and Tribological Behavior of Aluminum Matrix Composites Reinforced with In-Situ AlB_2 Particles, *Tribol. Int.*, 2016, **98**, p 41–47
39. K. Kalaiselvan, N. Murugan, and S. Parameswaran, Production and Characterization of AA6061-B_4C Stir Cast Composite, *Mater. Des.*, 2011, **32**, p 4004–4009
40. A.O. Adegbenjo, B.A. Obadele, and P.A. Olubambi, Densification, Hardness and Tribological Characteristics of MWCNTs Reinforced Ti_6Al_4V Compacts Consolidated by Spark Plasma Sintering, *J. Alloy. Comp.*, 2018, **749**, p 818–833
41. Z. Zhang, L. Zhang, and Y.W. Mai, Modelling Friction and Wear of Scratching Ceramic Particle-Reinforced Metal Composites, *Wear*, 1994, **176**, p 231–237
42. P.K. Rohatgi, S. Ray, and Y. Liu, Tribological Properties of Metal Matrix-Graphite Particle Composites, *Int. Mater. Rev.*, 1992, **37**, p 129–152
43. M. Moazami-Goudarzi, and F. Akhlaghi, Wear Behavior of Al 5252 Alloy Reinforced with Micrometric and Nanometric SiC Particles, *Tribol. Int.*, 2016, **102**, p 28–37

44. P. Xiao, Y. Gao, F. Xu, C. Yang, Y. Li, Z. Liu, and Q. Zheng, Tribological bEhavior of In-Situ Nanosized TiB_2 Particles Reinforced AZ91 Matrix Composite, *Tribol. Int.*, 2018, **128**, p 130–139
45. X.Y. Li, and T.K. Tandon, Mechanical Mixing Induced by Sliding Wear of an Al-Si Alloy Against M_2 Steel, *Wear*, 1999, **225–229**, p 640–648